


RESEARCH LETTER

Open Access



Probing shallow subsurface structures in the arc-continent collision suture zone near Hualien in Eastern Taiwan with magnetotelluric methods

Ping-Yu Chang^{1*} , Haiyina Hasbia Amaniah¹, Azhar Fikri², Jordi Mahardika Puntu¹, Ding-Jiun Lin¹, Chun-Hsiang Kuo¹, Chien-Ying Wang¹ and Wen-Yen Chang³

Abstract

We used the magnetotelluric method (MT) to investigate near-surface structures at the northern end of the Longitudinal Valley in Hualien City, eastern Taiwan. This valley is considered the suture zone of the arc-continent collision between the Eurasian plate and the Philippine Sea plate, making it crucial to understand the geological settings at its northern end. We conducted MT measurements along the L2 and L3 lines on the north and south sides of the city, respectively. On the L2 survey line to the north of Hualien City, our inverted image indicates that the Tananao metamorphic complex, with a resistivity of several hundred ohm-m, is in vertical contact with sedimentary rock with a resistivity higher than 1000 Ω -m. This vertical contact zone is consistent with the distribution of the Beipu fault. However, the vast area between L2A and L2E is occupied by airports and military facilities, making it challenging to lay out survey stations to clearly analyze critical regional structures such as the Beipu and Milun faults. The 2D inversion results of the L3 are consistent with past reflection seismic interpretation results. The resistivity of the metamorphic Yuli Formation, which belongs to the continental basement rock in the west, is less than 200 Ω -m. Its top dips eastward, reaching depths greater than 2.5 km at the eastern end of the L3. The rocks above the metamorphic bedrock, composed of material with a resistivity greater than 1000 Ω -meters, are likely to be sedimentary rocks of the foreland basin. The difference in geological structure between the two survey lines, L2 and L3, may suggest the possible existence of an E-W orienting fault structure in the urban area between the two survey lines. Additionally, the rapid thickening of sedimentary rocks north of Hualien City may provide indirect evidence for the detachment model proposed by Shyu et al. (*Tectonophysics* 692:295-308, 2016). Further studies are required to resolve the resistivity structures and fault orientations in the urban region between the two survey lines.

Key points

1. MT methods were used to resolve the shallow structures in the collision suture zone in Eastern Taiwan.
2. The results show that the continental metamorphic rocks have a resistivity less than 1000 Ω -m.
3. The rocks that have a relative higher resistivity over 1000 Ω -m may be the sedimentary rocks belonging to the foreland settings.

*Correspondence:

Ping-Yu Chang
pingyuc@ncu.edu.tw

Full list of author information is available at the end of the article



© The Author(s) 2023. **Open Access** This article is licensed under a Creative Commons Attribution 4.0 International License, which permits use, sharing, adaptation, distribution and reproduction in any medium or format, as long as you give appropriate credit to the original author(s) and the source, provide a link to the Creative Commons licence, and indicate if changes were made. The images or other third party material in this article are included in the article's Creative Commons licence, unless indicated otherwise in a credit line to the material. If material is not included in the article's Creative Commons licence and your intended use is not permitted by statutory regulation or exceeds the permitted use, you will need to obtain permission directly from the copyright holder. To view a copy of this licence, visit <http://creativecommons.org/licenses/by/4.0/>.

4. The Beipu fault may be the contact between the continental metamorphic rocks and foreland settings.
5. The subsurface structures are different between our two survey lines and suggest a further study is needed in the area.

Keywords Magnetotelluric, Collision, Near surface, Suture zone, Taiwan

Introduction

The magnetotelluric (MT) method was originally proposed by Tikhonov and Cagniard (Cagniard 1953; Tikhonov 1950). In the half century since its inception, important developments in formulation, instrumentation, and interpretation techniques have transformed the MT method into one of the most competitive geophysical methods available for the imaging of geological targets in the deep subsurface up to a hundred kilometers (Chang et al. 2020a). Together with the seismic exploration method, the MT method has thus become an important means by which researchers conduct deep geophysical exploration. In Taiwan, the MT method is also widely used in some crustal tectonic structures (Bertrand et al. 2009; Chen et al. 2007), shallow fault structures (Chang et al. 2020b; Chen and Chen 2000), and in volcanic and non-volcanic hydrothermal systems (Chang et al. 2014; Komori et al. 2014).

In this study, we used MT methods to investigate subsurface structures in the Hualien City area (Fig. 1), particularly at the northern end of the Longitudinal Valley, which is considered the suture zone of the arc-continental collision. However, the area’s subsurface structure remains poorly understood. In addition, a Mw6.4 shallow earthquake occurred off the coast of Hualien, causing the collapse of several multi-storey buildings and 17 deaths in 2018 (Jian et al. 2019; Lin et al. 2019; Yamada et al. 2020) in Hualien City. Surface ruptures accompanying the 2018 earthquake imply that complicated subsurface structures may be present along the Milun Fault in the northeastern part of the city’s urban area. Shortly after the earthquake, we completed two MT survey lines L2 and L3 from west to east on the north and south sides of Hualien City in 2019 (Fig. 2). Through the MT surveys that we conducted for this study, we intend to resolve subsurface geological

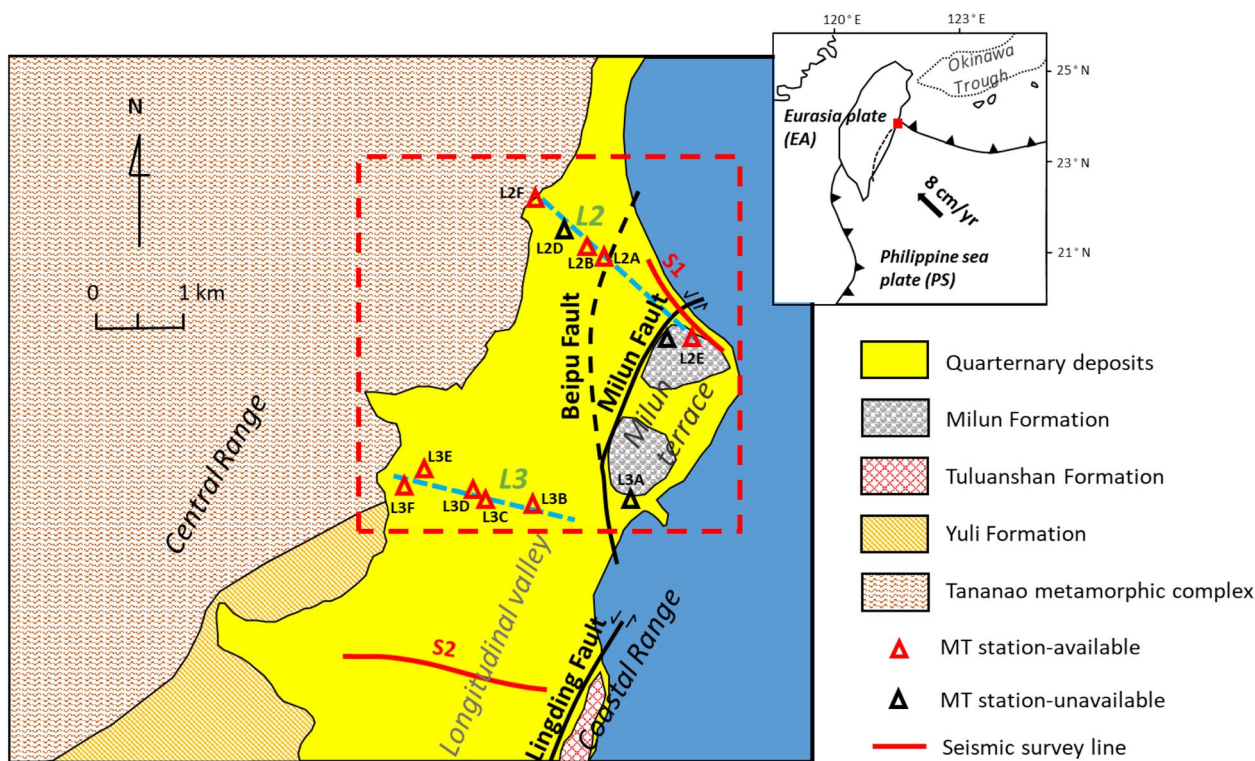


Fig. 1 The geological map in the Hualien City area. The square area shows our magnetotelluric study area corresponding to Fig. 2

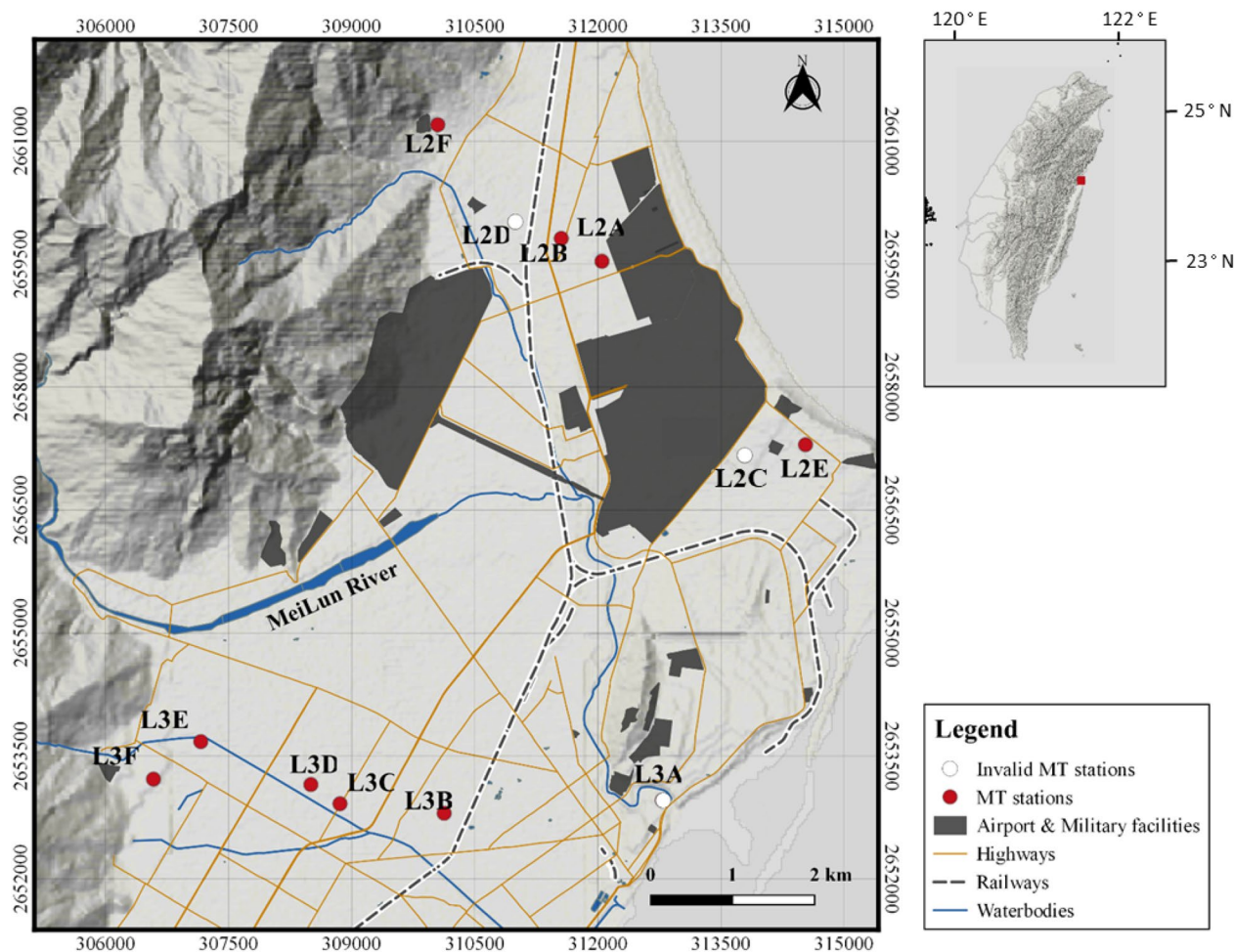


Fig. 2 Distribution of survey sites for preliminary magnetotelluric detection in Hualien City

structures and provide supporting data for further analysis of regional near-surface tectonics.

Geological settings

The eastern part of Taiwan is the boundary zone between the Philippine Sea (PS) plate and the Eurasian (EA) plate (Fig. 1). The Longitudinal Valley Fault (LVF) is considered to be the suture fault between the PS and EA plates. To the west of the Longitudinal Valley lies the Central Range, which consists mainly of metamorphic rocks on the EA plate. The eastern flank of the Central Range consists of rocks resulting from the arc-continent collision, such as gneiss, schists, slates, and meta-conglomerates. The Paleo-Mesozoic Tananao metamorphic complex, which consists of gneiss, marble, mica schist, black schist, and phyllite, can be observed in the Central Range on the west side of the study area. In addition, the Yuli Formation, which consists of meta-sandstone and green schists, can be observed on the southwestern corner of the study area. In addition, the Coastal Range to the east of the

Longitudinal Valley shows the relic island arc on the PS plate. The Coastal Range is located to the southeast of the alluvial plain and is comprised of two main formations: (1) the Tuluanshan Formation, made up of igneous rocks from the Late Miocene to the Early Pliocene, and (2) the Fanshuliao Formation, made up of Pliocene sedimentary rocks. Hualien City is located at the northern end of the Longitudinal Valley on the alluvial plain. The shallow subsurface of the alluvial plain is underlain by Holocene deposits consisting mainly of sands and gravels. The Milun Tableland rises from the alluvial plain in the northeastern part of Hualien City. The Pleistocene Milun Formation, which mainly consists of conglomerates, with some coral-reef and Quaternary sand and mud deposits, forms the topmost layer of the Milun Tableland.

The 8-km-long Milun fault (Lin 1962) extends in a north-south direction along the western margin of the Milun Tableland, and is interpreted as a left-lateral strike-slip fault with a reverse slip component (Hsu et al. 2019). The NNE-trending Lingding Fault, the northernmost

segment of the LVF, is located in the southeast region of Hualien City along the foothills of the Coastal Range, and exhibits a left-lateral displacement with a reverse component (Chen et al. 2008). The Beipu fault structure, although with no field evidences found at the ground surface and only interpreted by the GPS measurements, is thought to be an active fault similar to the Milun Fault (Yen et al. 2011) and is located on the northwest side of Hualien City. The alluvial plain on the western side of the Beipu fault (Shih et al. 1983) is slightly tilted toward the northeast, while the Meilun River along the fault developed abnormal geomorphic features (Fig. 1), which are thought to be related to the long-term movement of the Beipu Fault (Yen et al. 2011).

On February 6, 2018, the aforementioned earthquake of Mw 6.4 occurred 18 km northeast of Hualien city, resulting in 17 deaths and 285 injuries. The 2018 Hualien earthquake is believed to have taken place at the northern extension of LVF (Toyokuni et al. 2021) off the coast of Hualien. Researchers found that major surface ruptures occur along the Milun Fault, which runs between the urban area and the Milun Tableland (Hsu et al. 2019; Wu et al. 2019; Yamada et al. 2020). The 2018 earthquake and its aftershocks affecting the surface-level shear ruptures extend across part of the city, from the Milun Fault to the northern end of the Lingding Fault. This area is located in the transition regions where the collision suture zone enters the Ryukyu subduction zone. However, there has been no detailed underground geological exploration research in the past. Lin et al. (2021) proposed that the origin of the Milun Tableland and the southern Hualien ridge may be an uplift wedge structure caused by the oblique collision of the Philippine Sea plate in the north-west direction. Shyu et al. 2016 explain the mechanism of the uplifted wedge structure to the tectonic settings with

a detachment model. This study intends to use high-resolution near-surface geophysical surveys to help clarify the regional geological settings, and to verify the aforementioned model assumptions (e.g., Lin et al. 2021; Shyu et al. 2016).

Instruments, configurations, and data processing

Using advanced sensor and logger technologies, researchers have recently been able to collect MT data (Haberland and Ritter 2016; Schulze et al. 2023). We used the three-axis fluxgate magnetometers Bartington™ Mag-639 and Mag-03MS to measure magnetic fields. The magnetic sensor Mag-03MS can identify noise levels down to < 12pTrms/√Hz at 1 Hz and a bandwidth from DC to 3 kHz. The broadband Mag-639 sensor has a bandwidth from DC up to 12 kHz and noise levels less than 20 pTrms/√Hz at 1 Hz. Lead–lead chloride (Pb–PbCl₂) non-polarized electrodes are used as electric-field sensors because they are more efficient and produce less noise than copper–copper sulfate non-polarized electrodes. As illustrated in Fig. 3, we adopted the X-configuration with 4 electrodes spread approximately 60 m apart in an X-shaped configuration, where 2 electrodes are situated in the north–south direction, and the rest are aligned in the east–west direction (Simpson and Bahr 2005). We added bentonite slurry to the holes in which the non-polarized electrodes were buried. The addition increased the coupling of the sensors to the ground.

In the study, we used the Earth Data™ EDR-210 dataloggers. Sampling frequencies can be set from 1 Hz to 3000 Hz to record measurements through six independent channels. The individual EDR-210 datalogger is also equipped with GPS satellite synchronization timing and a built-in solid-state hard disk to record a large amount of data. With the power supply from a 12 V battery, the

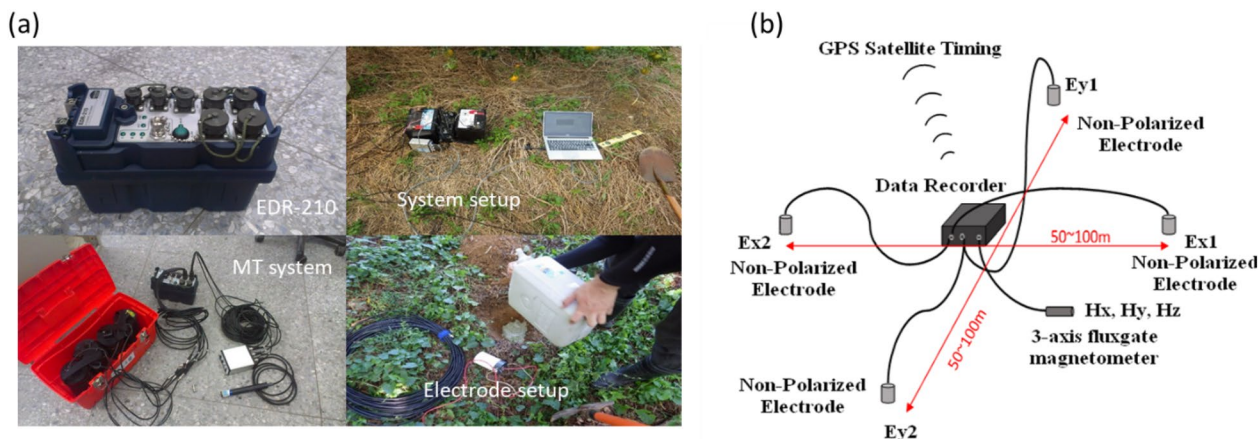


Fig. 3 Upper: Schematic diagram of our field survey and the deployment of our self-assembled simultaneous-sequence magnetotelluric instrument. Lower: the magnetotelluric system used in this study

datalogger can record MT data for at least seven days in the field. We deployed the system for 48 to 72 h with a sampling frequency of 500 Hz. When conducting the two-dimensional survey, the optimal site separation should be less than the targeting skin depth. In our study, the sites are located at a separation distance of 1–1.5 km in general with regard to the available deploying space in the city, since our targeting depth is 2–3 km.

Owing to the high noise level in the urban area and malfunction problems affecting a datalogger, we obtained analysable measurements from only 4 sites in L2 and from 5 sites in L3. After examining the raw records, we decided to select only the time period from 12 to 4 am for further processing, since there are fewer electromagnetic noises during this time period than at other time periods in the urban area of Hualien City. To remove the domestic power-line signals, we used a notch filter to filter out noises around the 60-Hz level. To help process the data, we used the Bounded Influence Remote Reference Processing (BIRRP) program (Chave and Thomson 2003) along with open-source MT processing python code, MTpy (Krieger and Peacock 2014). In this way, we sought to gain insights into the impedance, apparent resistivity, and phase angles of the measured electromagnetic fields. Finally, we inverted the processed data with the freeware Occam2D (de Groot-Hedlin and Constable 2004) to build up the two-dimensional resistivity models for further analysis.

Results

The raw time series

Because the study area was in an urban area, we had to account for possible artifacts from urban activities that can saturate our measurements with noisy signals, especially during the daytime hours. After reviewing the data, we decided, as noted above, to focus only on the measurements from the midnight hours, specifically between 0000 (zero hundred) hours and 0400 (zero four hundred) hours, because this four-hour stretch contains the least amount of noise of any four-hour period. Figure 4 presents the raw time series and time spectrum diagrams of the L3E site during the 0000–0400 period on July 5, 2018, with all data collected on the basis of the aforementioned MT instruments. At the midnight hour, the electric fields ranged from about -500 to 500 mV/km in both the northward (X-) and eastward (Y-) directions. The magnetic fields ranged from -40 to 40 nT and from -20 to 20 nT in the X- and Y-directions, respectively. The variation in the strength of the northward magnetic field was about twice as great as the corresponding eastward variation. These findings are consistent with those presented in Chang et al. (2020c) regarding the eastern part of Taiwan and based on similar instruments. In addition,

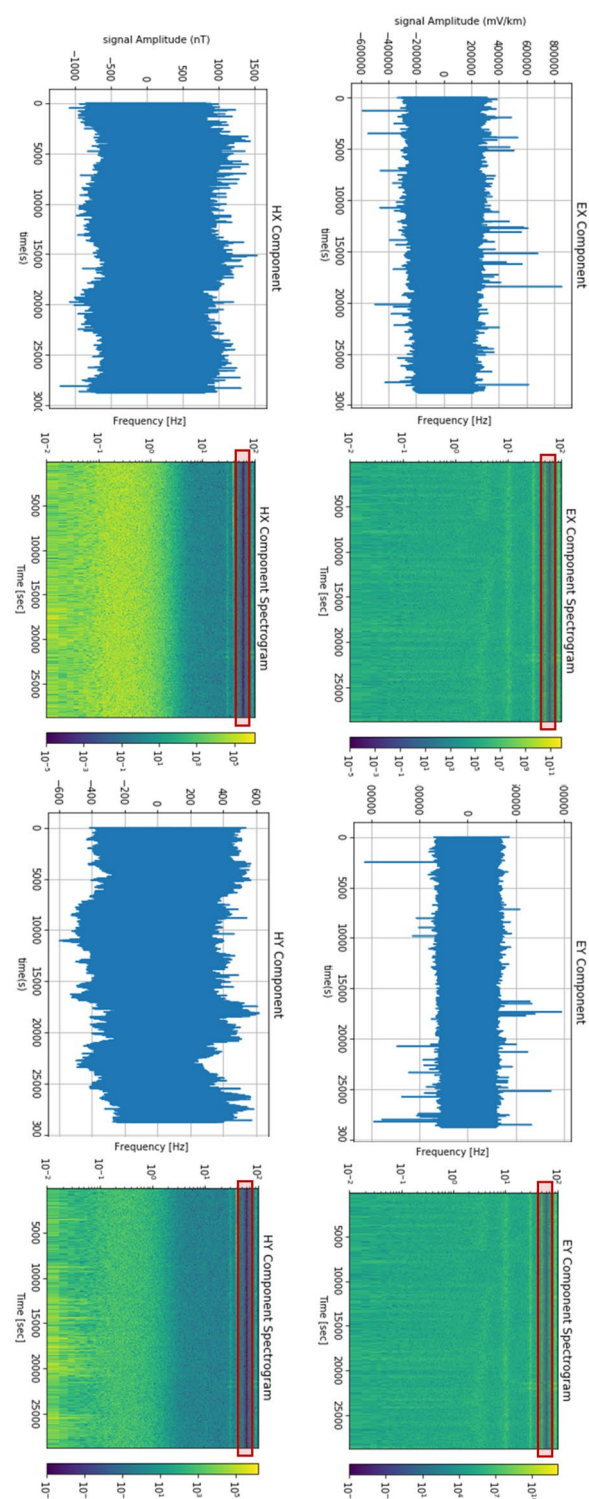


Fig. 4 The electric field time series and the time-spectrum diagram of the **a** Ex, **b** Ey, **c** Hx, and **d** Hy fields

power-line noise at 60 Hz was observable at the midnight hour in both the electric and magnetic fields, as is noted in Fig. 4’s time-spectrum diagram (indicated by a red rectangle). Of course, the power-line noise was much weaker during this time period than during daytime periods. Most of the energy strength of electric and magnetic fields was concentrated in the low-frequency part of the spectra. Random pulse-like noises can also be found in the time-spectrum diagrams. Thus, we had to adopt the remote reference method mentioned in Gamble et al. (1979) and use it with the synchronized data collected at different sites. In this way, we reduced the random noises in our analysis involving MT measurements.

The processed apparent resistivity and phase data

From the geological settings, we learned that the Longitudinal Valley and regional tectonic structures, such as the Milun and Lingding Faults, are mostly striking at about N40°E. We rotated our estimated impedance tensor by 40°, and calculated the apparent resistivity and phases regarding the rotated impedance. Figure 5 shows the strikes of the calculated apparent resistivities and the long axis direction of the calculated phase tensors of the measurements. It appears that most of the resistivity features are parallel or perpendicular to the rotated principle axis. In theory, the phases would become dimensionless if one rotates the coordinates so that they are aligned with the regional structure orientation. Yet, we observed that the phases have an additional dominating orientation in an almost east–west direction, which may stem from the effects of the conductive ocean in the east. We then calculated the apparent resistivity in two induction modes: the transverse electric (TE) mode and the

Table 1 Basic information from the magnetotelluric survey sites in Hualien City

Site	Latitude	Longitude	Elevation (m)	Ex-length (m)	Ey-length (m)
L2A	24.03951	121.61006	19	53.9	75.8
L2B	24.04205	121.60520	2	51.7	68.9
L2C	24.01804	121.62705	35	53.7	42.3
L2D	24.04389	121.59967	10	43.1	59.6
L2E	24.01921	121.63435	31	91.2	89.6
L2F	24.05463	121.59046	79	42.7	57.4
L3A	23.98012	121.61702	14	57.5	61.7
L3B	23.97879	121.59088	20	90.5	43.9
L3C	23.97989	121.57841	31	59.7	38.5
L3D	23.98201	121.57493	35	67.8	55.8
L3E	23.98679	121.56177	52	55.9	80.3
L3F	23.98268	121.55608	124	64.2	60.8

transverse magnetic (TM) mode. The TE mode consists of the inputs of the Ex and Hy channels, whereas the TM mode uses the inputs of the Ey and Hx channels. The TE mode describes when the current is induced and flows along the strike, and the TM mode describes when the current flows across the strike. Thus, the TE mode tends to be sensitive to conductive bodies, and the TM mode tends to be sensitive to resistive bodies.

We discovered that the apparent resistivity and the phases can experience a distinct distortion at frequencies higher than 1 Hz in the L2A site. There are also negative phases for frequencies higher than 1 Hz at most of the sites for both the TM and TE modes. These results perhaps reflect the coastal current channelling at the

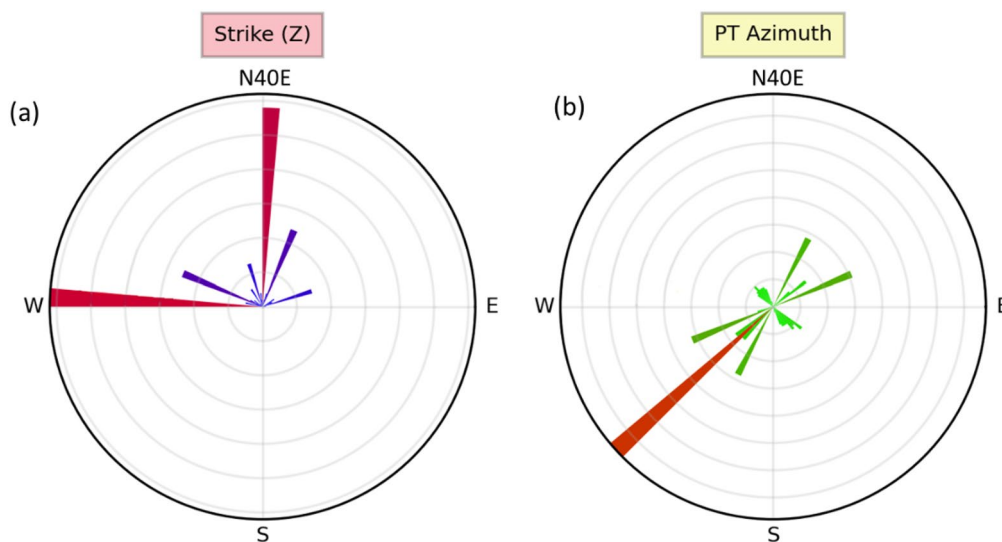


Fig. 5 Left: the strikes of the calculated apparent resistivities. Right: the long axis direction of the calculated phase tensors of the measurements

conductive boundary (e.g., Constable et al. 2009; Fischer et al. 1978; Key and Constable 2011; Schwalenberg and Edwards 2004; Selway et al. 2012; White and Heinson 1994). As a result, we decided to use only the data at frequencies higher than 1 Hz to avoid contamination from coastal effects (Table 1).

Figure 6 shows the processed apparent resistivities and phases of the survey sites, L2A, L2B, L2E, and L2F on the L2 line in the TM and TE modes, respectively. To process the L2A and L2B sites, we used L2F as the reference site. We processed L2E and L2F using L2B and L2A as the reference sites, respectively.

In Fig. 6a, the apparent resistivity of the TM mode of the L2 sites varies between 10^2 and 10^4 Ohm-m. The L2A and L2B sites exhibited a similar trend in the apparent resistivity of the TM mode, while the L2E and L2F sites have similar TM resistivities for frequencies higher than 7 Hz. The resistivities at the L2B and L2F sites decreased from over one thousand Ohm-m to several hundred Ohm-m for frequencies extending from 5 to 1 Hz. The resistivities of L2A and L2E gradually increased with the decreasing frequency to nearly 4000 Ohm-m at 1 Hz. The phases at the L2 sites exhibited an increasing trend when the frequency decreased in the TM mode. The L2B and L2F sites exhibited a similar trend in the phase variation, and the phase variation of the L2A site was similar to that

of the L2F site. Figure 6b shows the apparent resistivity and phases of the L2 sites in the TE mode. On average, the TE mode's apparent resistivity was about an order of magnitude lower than the TM mode's. The L2A and L2B sites presented a similar trend, and the L2E site was similar to the L2F site regarding the TE mode's apparent resistivity at the frequencies higher than 7 Hz, as was the case in the TM mode. Yet the L2A site presented a trend quite different from the trend of the other sites, as the L2A site involved a steeper increase, from about 400 Ohm-m at 5 Hz to over 1000 Ohm-m at 1 Hz. The L2B and L2F sites exhibited a similar series of TE-mode changes. The differences among the TE modes at the L2E site were similar to those observed among the TM modes. The L2A site, however, may have been affected by a near-surface conductive body and may have had near-zero negative phases for the frequencies higher than 2 Hz.

Figure 7a shows the processed apparent resistivities and phases in the TM mode of the survey sites on the L3 line. The L3B, L3C, L3D, and L3E sites exhibited similar trends in the apparent resistivity of the TM mode. The resistivity of the four sites varied between several thousand Ohm-m and about 10,000 Ohm-m. The phase diagram of the L3 site presents an increasing trend in the TM phase when the frequencies decreased from 20 to 1 Hz. The TE apparent resistivity in Fig. 7b indicates that the L3B,

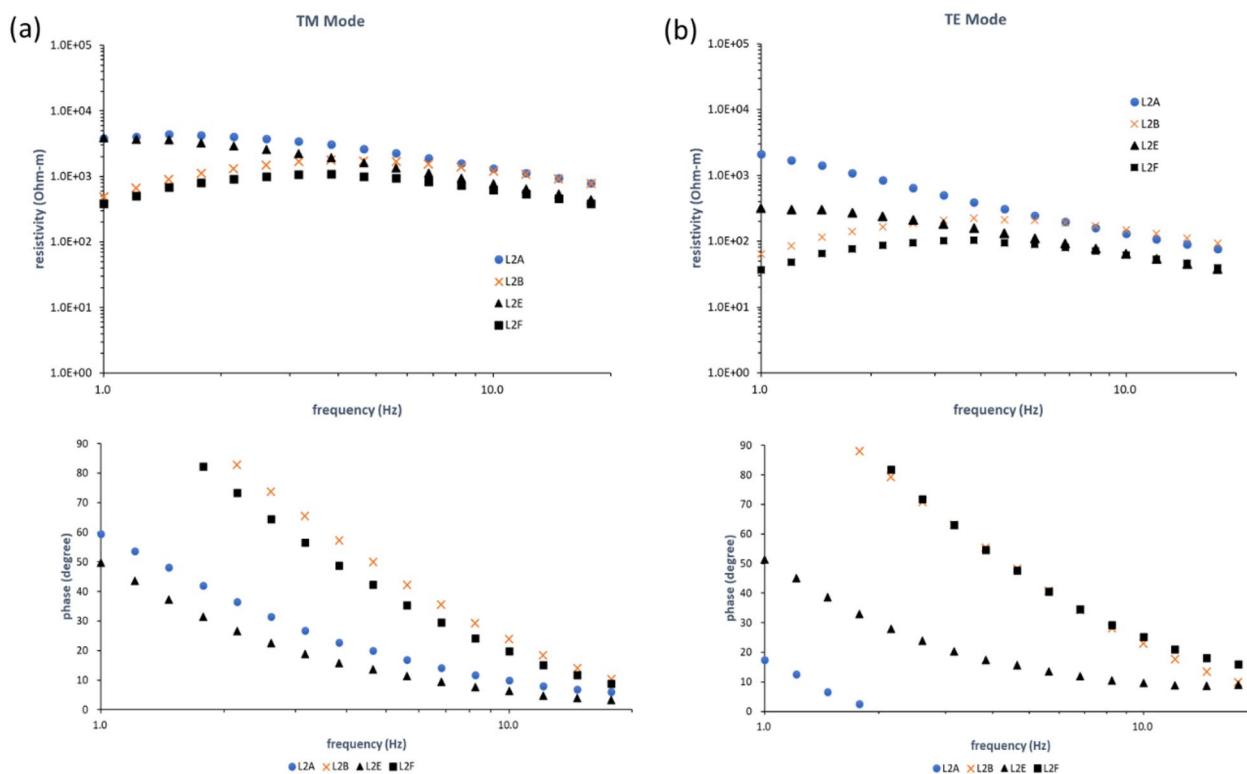


Fig. 6 a The TM apparent resistivity and phases for measurements at L2 sites. b The TE apparent resistivity and phases for measurements at L2 sites

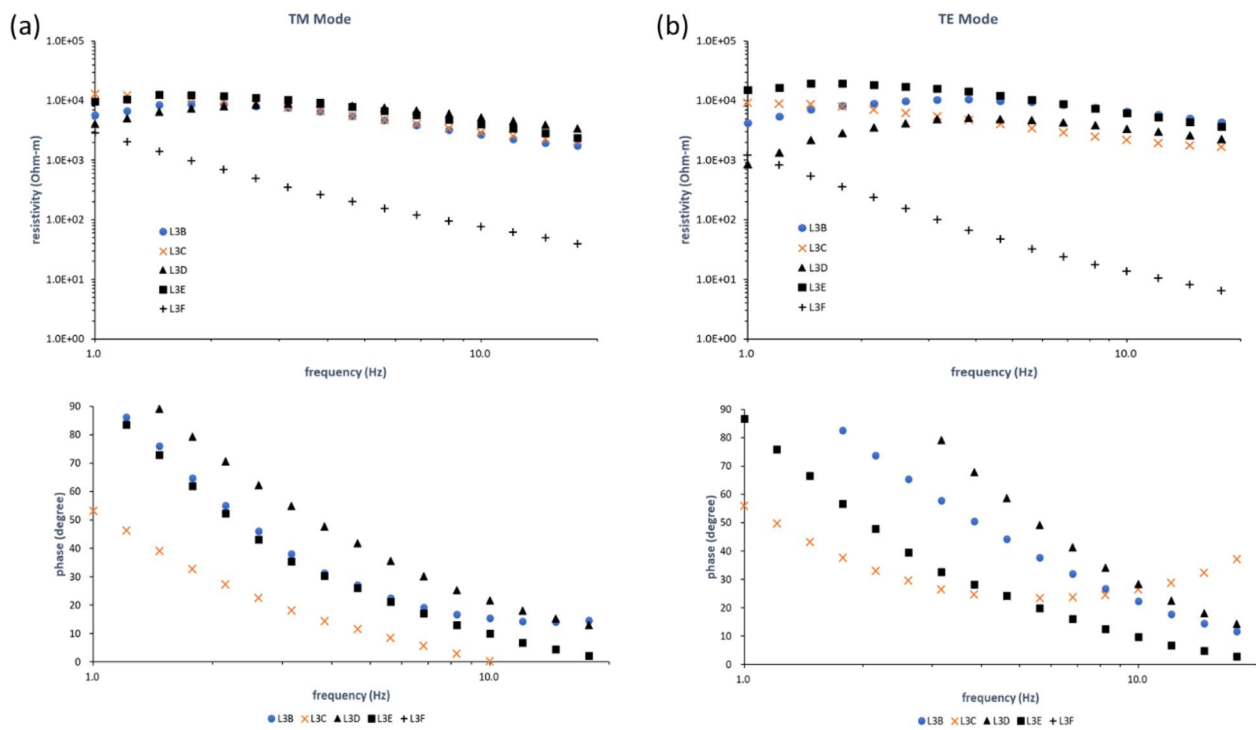


Fig. 7 **a** The TM apparent resistivity and phases for measurements at L3 sites. **b** The TE apparent resistivity and phases for measurements at L3 sites

L3C, L3D, and L3E sites had similar resistivity ranges, extending from 1000 Ohm-m to 10,000 Ohm-m. The TE resistivity increased when the frequencies decreased from 20 Hz to about 3 Hz, and then slightly decreased for frequencies less than 2 Hz for the L3B, L3D, and L3E sites. In contrast to the other three sites, the TE resistivity of the L3E site increased from about 3000 Ohm-m at 20 Hz to over 10,000 Ohm-m at 1 Hz. The TE resistivity of the L3F site, which increased from about 700 Ohm-m at 20 Hz to 1000 Ohm-m at 1 Hz, exhibited a distribution very different from those of the other sites on the L3 survey line. The findings may imply that the L3F is located in an area where the geology is quite different from the geology of the other L3 sites. The L3B, L3D, and L2E sites exhibited a similar TE phase trend. The TE phase of the L3C site decreased from around 40° at 20 Hz to 25° at 6 Hz, and then increased to about 55° at 1 Hz.

The inverted two-dimensional profiles

We used the Occam2D (de Groot-Hedlin and Constable 2004) code to invert the two-dimensional (2D) model for survey lines L2 and L3. We used the apparent resistivity of the TM measurements for the inversion, since the TM mode is more sensitive to the geological structures perpendicular to the survey line direction. We did not use the phase data for the inversion in this study because we found the phase exhibiting more coastal effects than the

apparent resistivity. Figures 8 and 9 show the profiles of the inverted 2D results based on the TM measurements for the L2 and L3 sites, respectively. The model fitting in relation to the root-mean-square (RMS) errors is about 17.8% for the L2 measurements, and is only about 15.4% for the L3 measurements.

In Fig. 8, the rock in the western part of the L2 profile exhibited relatively lower resistivity than in the eastern part at a depth greater than 500 m. The resistivity was mostly less than 1000 Ohm-m in the western part of the L2 profile, and was between 1000 and 10,000 Ohm-m for rocks deeper than 500 m in the eastern part of the profile. The L2F site on the western end of the L2 line is located at the base of foothills of the eastern Central Range, and the schists of the Tananao Complex can be observed at the nearby outcrops. Hence, we believe the area from L2F to L2A is mainly consisted of the schists of the Tananao Complex. For rocks at a depth between 1200 m and 2400 m deep at the L2F site, the resistivity was slightly higher than 1000 Ohm-m, which may be due to the resistive complex composition, such as marble or gneiss, in the Tananao Formation. Other than the deeper resistive rocks at the L2F site, the resistivity of rocks at the L2B and L2A sites was mostly few hundred Ohm-m and shows a same resistivity range as the rocks less than 1000-m deep at the L2F. In addition, the L2A site appeared to be near the boundary that separates the

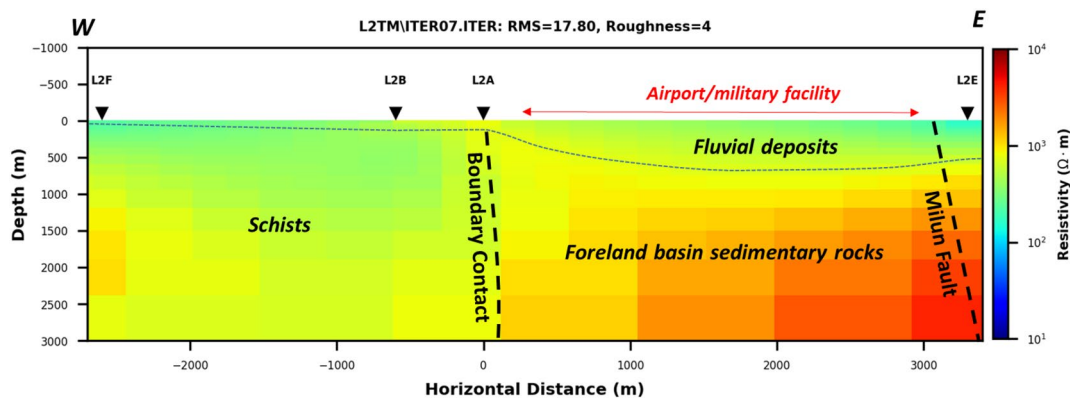


Fig. 8 The inverted image of the L2 survey line in the study area shows the dotted line indicating the boundaries between the layers of fluvial sediments and the underlying Tananao schists and foreland sedimentary rocks, with significant resistivity differences. The dashed line shows the possible fault structure in the study area

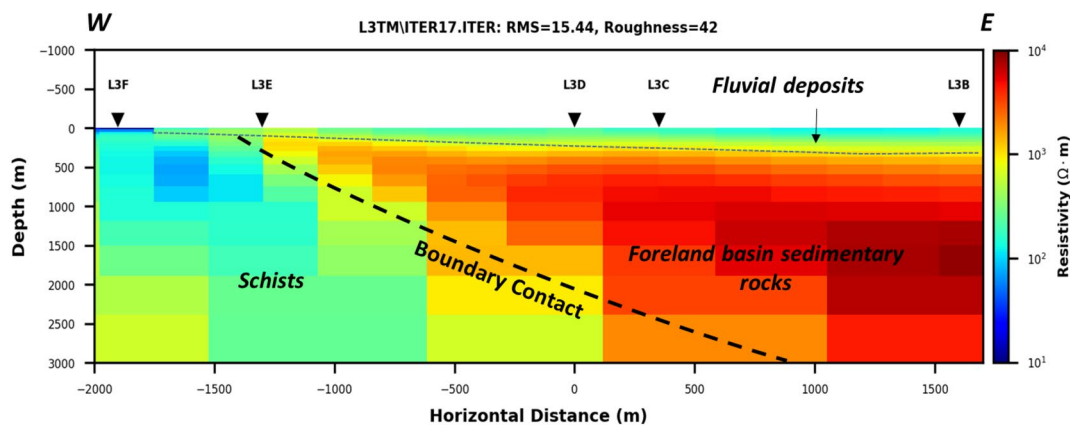


Fig. 9 The inverted image of the L3 survey line in the study area: the dotted line indicates the boundaries between the layers of fluvial sediments and the underlying schists and foreland sedimentary rocks, with significant resistivity differences

conductive schists from the resistive rocks in the eastern part of the L2 profile. The L2E site, on the other hand, consists of rocks and, in our measurements, had a resistivity much higher than 1000 Ohm-m at a depth greater than 500 m. The surface part of the L2E site consists of rocks with resistivity less than 1000 Ohm-m. The boreholes with a depth less than 200-m deep indicate that the shallow subsurface is mainly fluvial deposits consisted of sand and gravels (Chang 1994). The drilling findings near the L2E site have led us to conclude that the surface conductive layer may represent unconsolidated fluvial deposits dating from the late Pleistocene. In addition, previous studies have proposed that the Milun Fault and Beipu fault structure are located between the L2A and L2E sites. Unfortunately, we had no MT sites between the L2A and L2E sites because the area is occupied by the facilities and runways of the Hualien military airport. Thus, we have no further information about the exact

nature of the subsurface structures, especially the Milun Fault, and possible resistivity compositions between the L2A and L2E sites. However, the location of the possible Beipu Fault structure seems to be consistent with the vertical contact between the western Tanao schists and the eastern resistive rocks in the MT image. Previous resistivity studies in the Longitudinal Valley (e.g., Chen 1995; Chien 2015) suggest that the slates and foreland sedimentary rocks, such as conglomerates, outcropped at the eastern flank of the Central Range are often much more resistive than the schists and sedimentary rocks of the Coastal Range. Therefore, we think that the Beipu Fault structure may represent the major contact between the schists in Tananao metamorphic complex and the possible sedimentary rocks in the foreland basin between the two colliding plates. Figure 8 presentation of the Milun Fault and Beipu contact structure rests on our inferences from the currently available data. Further MT

exploration is needed to resolve the exact distribution and orientation of the Milun Fault and Beipu Contact in the airport area.

Figure 9 represents the inverted resistivity profile of the L3 line that located south of the Hualien City. Because the western end of L3 is located near the outcrop area of the Yuli formation comprised by mainly meta-sandstones and green schists, the conductive rocks under L3F may represent the Yuli formation. The subsurface strata shallower than 500-m between the L3E and L3B sites with resistivity less than 200 Ohm-m are interpreted as fluvial sediments comprised by primarily sand and gravel. We know this based on shallow boreholes within 200-m deep in the region. In addition, a layer with resistivity higher than 1000 Ohm-m can be observed between the L3E and L3B sites below the fluvial deposits and gradually gets thicker as one moves east (Fig. 9). Indeed, the thickness exceeds 2.5 km at the L3B site. Compared with results from regional resistivity surveys, this resistive layer may represent the slates and foreland sedimentary rocks that are similar to the conglomerates outcropped in the eastern part of the Central Range. In the L3 profile, the relatively conductive Yuli Formation and the overlying resistive sedimentary rocks exhibit an eastward-dipping angular contact. As can be seen in Fig. 9, we found the L3 profile exhibits quite different framework to that of the L2 profile in Fig. 8. We will discuss the possible implication of L2 being different from L3 in the following section.

Discussion

In our study, we found that measurements with a frequency lower than 1 Hz resulted in a negative phase. Thus we had to use only data with frequencies higher than 1 Hz to probe near-surface structures. Because we conducted our surveys near the ocean, we inevitably had to deal with coastal effects on our MT measurements. Thong (2008) proposed that eastern Taiwan's coast would affect measurements with frequencies lower than 0.1 Hz. In our study, we found that coastal effects may have also affected data involving frequencies lower than 1 Hz. Therefore, one should be careful when carrying out MT surveys near oceans, whose coastal effects can distort data, rendering it unusable. In addition, we noticed that our estimated phases failed to provide stable and consistent results for the inversion. However, we could manage to use only the apparent resistivity data for the 2D inversion. Coastal effect as well as the urban culture noise that having a greater influence in our phase estimation, may explain the bad estimation results in the phase. In the future, we will try to conduct three-dimensional forward modelling that involves the coastal effect and possibly the urban noises to verify our findings.

Verification of the results and interpretations of our analytical study is critical for the MT profiles of the L2 and L3 sites. However, restrictions imposed by both the airport and urban areas have prevented researchers from conducting seismic reflection surveys with sufficient penetration depths in the study area, especially near the L2 line. Two seismic survey lines have been completed in the nearby area, as shown in Fig. 2. The S1 survey line is from the MiDAS project database (https://e-dream.tw/midas_project/) and is located primarily along the northern coastal line of the Milun Tableland. The S2 line is located to the south of Hualien City (Shie 2017) and is about 4 km away from L3. The original seismic profiles with wiggle traces were re-interpreted in this study to be compared with our MT profiles. We picked the positive and negative peaks from the wiggle traces and traced their horizontal extension to the adjacent traces for picking reflectors. Envelopes of the reflectors were then evaluated along the depth, and the boundaries were marked between different patterns of envelope trending. We also registered truncation of the reflector envelopes to identify possible high-angle faults or fractures. Using these approaches, we identified three and four major rock units in the S1 and S2 profiles, respectively. Compared to the regional geology and shallow boreholes, we suggest a geological interpretation for the two seismic profiles. Figure 10a, b present the geological interpretation of the S1 and S2 seismic profiles, respectively.

The Milun Table 1 and in the S1 profile is mainly composed of conglomerates, and the seismic profile shows many short and discontinuous reflectors. In addition, there seems to be a contact that separates discordant reflector settings of the conglomerates and rocks below the contact. In the eastern flank of the Central Range, the rocks include schists, slates, and conglomerates from west to east (CGS 2023). Also, the Milun conglomerates are outcropped on the Milun Tableland, composed of boulders of slates, quartzite, and schists that are from the Central Range. Therefore, we refer to the rocks below the conglomerates as the foreland sedimentary rocks in Fig. 10a based on the geological settings in the area. However, this assumption needs to be verified in future studies since there are no boreholes that reach this depth at present. On the west side of S1, Quaternary sediments were deposited horizontally on folded sedimentary rocks and rapidly thickened westward to about 600 m thick. Unfortunately, the S1 seismic survey line overlaps with our L2 line by only about 2 km, and most of the overlapping part is in the airport, where we were unable to deploy the MT stations. Therefore, it is difficult to compare the S1 profile with the L2 results directly. Yet

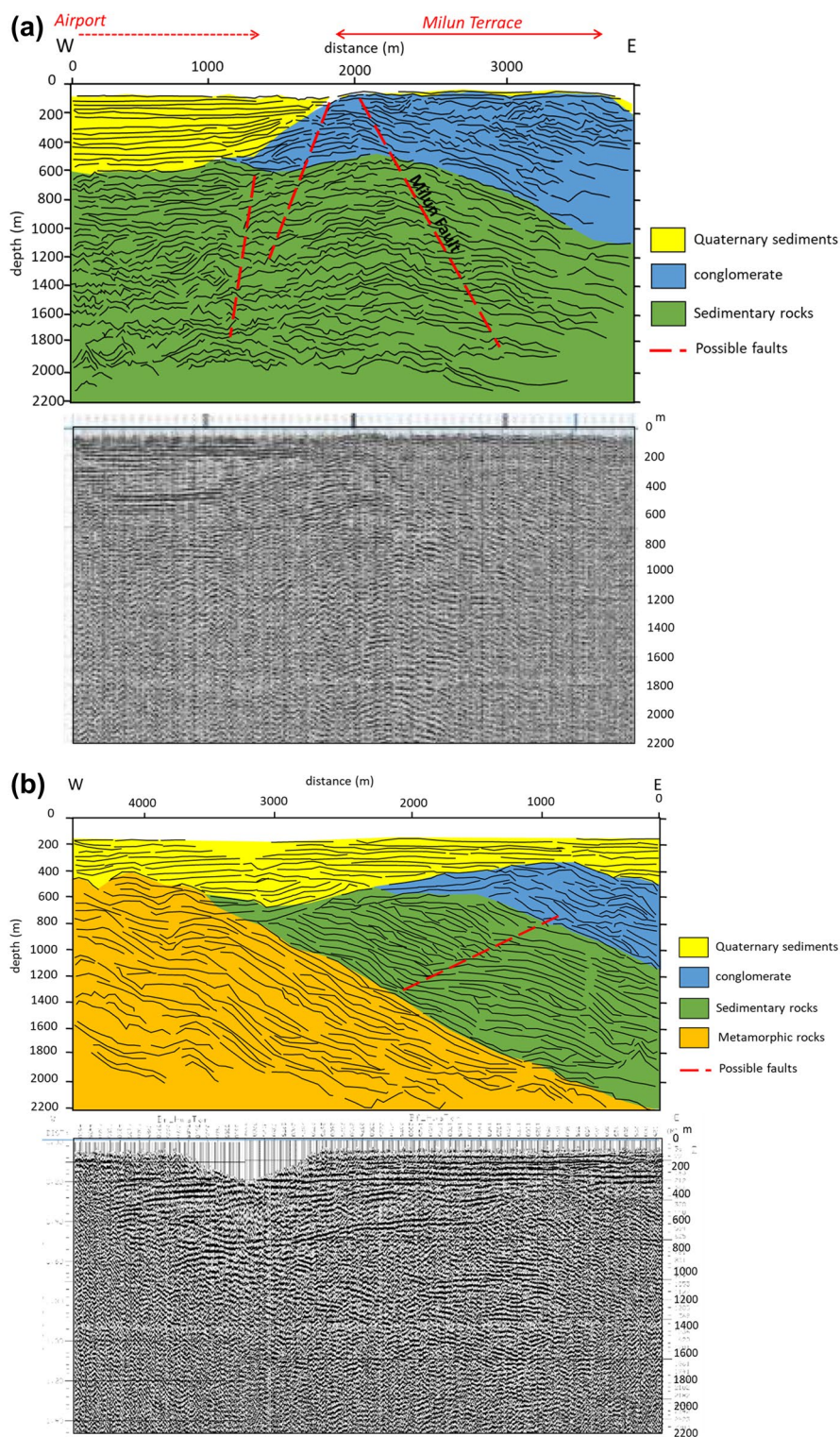


Fig. 10 **a** Lower: The seismic reflection profile for the S1 survey line from the MIDAS project database (https://e-dream.tw/midas_project/). Upper: The interpretation of the seismic reflection profile and explanations for the S1 line. **b** Lower: The seismic profile for the S2 survey line by Shie (2017). Upper: The re-interpreted profile that shows the picked reflection profile surfaces and interpretation explanations. Red dashed lines indicate the possible faults depicted from the discontinuities of the reflection surfaces

the contact between the Quaternary sediments and the sedimentary rocks is still consistent with that in the MT results of the L2 line.

On the other hand, although the S2 seismic profile is about 4 km from the L3 line, the two profiles exhibit similar geological structures. We identify a contact between the schists of the Yuli Formation and the overlying rocks that may suggest possible sedimentary rocks or conglomerates. The contact dips to the east with an angle of about 40° to 50° in the S2 profile, which is consistent with our MT findings for the contact between the conductive schists and the foreland sedimentary rocks. Above the schists, the rock settings were divided into three groups: the lower sedimentary rocks with open antiform reflectors, the upper conglomerates with gentle antiform reflectors, and the fluvial sediments with mostly horizontal reflectors. It should be noted that the seismic interpretation is based on regional geology and requires verification in the future through deep boreholes in the study area.

Compared with the southern L3 profile, the metamorphic rocks and sedimentary rocks present a high-angle contact in the profile of the L2 survey line. However, without deploying MT survey sites in the “gap” area occupied by the airport and the military base, we are not able to verify the actual morphology of the contact. Based on our current results, the high-angle contact in the L2 line is consistent with the Beipu fault structure that has been identified with the topography (Shih et al. 1983) and GPS observations (Yen et al. 2011). Although the Beipu fault was considered a minor fault in the past and was ignored, we find that the Beipu fault represents an important contact between the schists of the Tananao complex and the foreland sedimentary rocks.

Shyu et al. (2016) have proposed a detachment structural model for the development of the northernmost Longitudinal Valley. The foreland sedimentary deposits detached from the subducting plate and formed the squeezing-up Milun Tableland. Their model includes thickening “soft” sedimentary rocks, which are detached from the subducting bedrock and overthrusting northward and westward at the northern end of the Longitudinal Valley. Our findings from the magnetotelluric and seismic results support the model proposed by Shyu et al. (2016). Foreland sedimentary rocks are in contact with metamorphic rocks at a lower angle on the south side of Hualien City, while in the north of Hualien City, the vertical thickness of sedimentary rocks is thickened and they are in contact with Tananao schists at a nearly vertical angle across the Beipu fault.

Conclusions

In this study, we conducted Magnetotelluric surveys in the eastern Taiwanese city of Hualien to investigate the resistivity structures and fault orientations of the area. Our surveys were conducted at twelve sites along two lines, L2 and L3, located at the northern and southern part of the city. We inverted only the apparent resistivities whose frequencies were higher than 1 Hz and collected measurements during the night hours to reduce the MT’s coastal distorting effect on phase data and human artifacts.

Our 2D inversion results show that the resistivity images of the L2 and L3 profiles are quite different. The L2’s western part consists of the Tananao metamorphic complex with a resistivity less than 1000 Ohm-m, while the L2’s eastern part mainly consists of rocks, most likely the foreland deposits, with resistivities higher than 1000 Ohm-m at a depth greater than 500 m. The rocks forming the Tananao metamorphic complex are in vertical contact with the resistive foreland sedimentary rocks, and the surface location of the contact corresponds to the Beipu fault near the L2A site. The Milun Fault is another major active structure besides the Beipu fault, but unfortunately, we were unable to verify its location due to the absence of sites in the vast area between the L2A site and the L2E site, which is occupied by a large airport and military facilities.

On the other hand, there is good agreement between the L3 data and the data from the seismic surveys completed at a survey line about 4 km south of the L3 line. The schist basement with resistivity less than 200 Ohm-m dips toward the east and may reach a depth of over 3 km at the L3B site. A resistive layer with resistivity higher than 1000 Ohm-m lies over the conductive schists, with a contact dipping to the east. We interpreted the resistive layer as possibly consisting of sedimentary rocks belonging to the foreland setting.

The difference in the structural settings between the L2 and L3 lines implies that possible structures may exist at the urban area between the two survey lines. Instead of the Milun fault that has gained a lot of scientific attention, this study shows that the urban area of Hualien city may be a key area in resolving the regional tectonics related to the arc-continent collision. A series of geological boreholes deeper than 500 m in the urban area may be necessary for this purpose. In future research, we plan to deploy more MT sites in the gap area between the L2 and L3 lines and the areas occupied by the airport and military facilities to better image the resistivity structures and fault orientations.

Acknowledgements

The present study has been funded by the Ministry of Science and Technology, Taiwan. We are thankful for the help of field crews in the near-surface

lab in the Department of Earth Sciences at National Central University. We also extend our thanks to the anonymous reviewers, who provided us with constructive suggestions and comments.

Author contributions

PC conceptualization, methodology and draft manuscript; HA and AF processing data, conceptualization, review and modify, and validation; JP, DL & CK methodology, review and editing; CW and WC seismic surveys and profile explanation.

Funding

The study was funded by the Ministry of Science and Technology, Taiwan, under the Project No. 108-2116-M-008-018.

Availability of data and materials

The data are available upon request to the authors.

Declarations

Competing interests

The authors declare that they have no competing interests.

Author details

¹Department of Earth Sciences, National Central University, Zhong-li, Taiwan. ²Department of Chemical Engineering, Institut Teknologi dan Bisnis Muhammadiyah Banyuwangi, Banyuwangi, Indonesia. ³Department of Natural Resources and Environmental Studies, National Dong Hwa University, Hualien, Taiwan.

Received: 20 August 2022 Accepted: 20 June 2023

Published online: 03 July 2023

References

- Bertrand EA, Unsworth MJ, Chiang CW, Chen CC, Wu F, Türkoğlu E, Hsu HL, Hill G (2009) Magnetotelluric evidence for thick-skinned tectonics in central Taiwan. *Geology* 37(8):711–714
- Cagniard L (1953) Theory of magnetotelluric method of geophysical prospecting. *Geophysics* 18:605–635
- CGS, 2023, National geological data warehouse, Vol. 2023, Central Geological Survey, MOEA.
- Chang S-J (1994) Investigation of subsurface geological structure of Hualien City region by shallow reflection seismic method [Master: National Central University].
- Chang P-Y, Lo W, Song S-R, Ho K-R, Wu C-S, Chen C-S, Lai Y-C, Chen H-F, Lu H-Y (2014) Evaluating the Chingshui geothermal reservoir in northeast Taiwan with a 3D integrated geophysical visualization model. *Geothermics* 50:91–100
- Chang P-Y, Goto T-N, Hu X, Um E (2020a) A review of electromagnetic exploration Techniques and their applications in East Asia. *Terr Atmos Ocean Sci.* <https://doi.org/10.3319/TAO.2020.11.05.01>
- Chang P-Y, Hsu H-L, Lin D-J, Fikri A, Puntu JM (2020b) Characteristics of electromagnetic Taiwanese-Railway signals and the signals' influences on magnetotelluric measurements. *Terr Atmos Ocean Sci* 31:589–601
- Chang P-Y, Ho G-R, Chen C-C, Hsu H-L, Chen C-S, Yeh E-C (2020c) An analysis of the subsurface fault systems with audio-magnetotelluric surveys in the western Ilan Plain of NE Taiwan. *Terr Atmos Ocean Sci.* <https://doi.org/10.3319/TAO.2020.02.17.01>
- Chave AD, Thomson DJ (2003) A bounded influence regression estimator based on the statistics of the hat matrix. *J R Stat Soc C Appl Stat* 52(3):307–322
- Chen C-S (1995) TEM mapping along the longitudinal valley in Eastern Taiwan and their tectonic implications. *Terr Atmos Ocean Sci* 6(2):271–283
- Chen C-S, Chen C-C (2000) Magnetotelluric soundings of the source area of the 1999 Chi-Chi earthquake in Taiwan: evidence of fluids at the hypocenter. *Terr Atmos Ocean Sci* 11(3):679–688
- Chen CS, Chen CC, Chiang CW, Shu HL, Chiu WH, Unsworth MJ, Bertrand EA (2007) Crustal resistivity anomalies beneath central Taiwan imaged by a Broadband Magnetotelluric Transect. *Terr Atmos Ocean Sci* 18(1):19
- Chen WS, Lin I-C, Yen Y-C, Yang C-C, Chi C-Y, Huang N-W, Lin C-W, Lin W-S, Hou C-S, Liu Y-C, Lin Y-H, Shih T-S, Lu S-T (2008) Fault segmentation of the Longitudinal Valley Fault in Eastern Taiwan: evidence from paleoseismic investigations and GPS observations. *Spec Publ Cent Geol Surv* 20:165–191
- Chien L-K (2015) An electric resistivity study of the faults in the taitung longitudinal valley, Eastern Taiwan. [Ph.D.: National Central University, p 81 p.
- Constable S, Key K, Lewis L (2009) Mapping offshore sedimentary structure using electromagnetic methods and terrain effects in marine magnetotelluric data. *Geophys J Int* 176(2):431–442
- de Groot-Hedlin C, Constable S (2004) Inversion of magnetotelluric data for 2D structure with sharp resistivity contrasts. *Geophysics* 69(1):78–86
- Fischer G, Schnegg P-A, Usadel K (1978) Electromagnetic response of an ocean-coast model to E-polarization induction. *Geophys J Int* 53(3):599–616
- Gamble TD, Goubau WM, Clarke J (1979) Magnetotellurics with a remote magnetic reference. *Geophysics* 44(1):53–68
- Haberland C, Ritter O (2016) GIPP: Geophysical instrument pool Potsdam. *JLSRF* 2:64
- Hsu Y-C, Chang C-P, Yen J-Y, Kuo-Chen H, Wang C-C (2019) Investigating the structure of the Milun fault from surface ruptures of the 2018 Hualien earthquake. *Terr Atmos Ocean Sci* 30:1–14
- Jian PR, Hung SH, Meng L (2019) Rupture behavior and interaction of the 2018 Hualien earthquake sequence and its tectonic implication. *Seismol Res Lett* 90(1):68–77
- Key K, Constable S (2011) Coast effect distortion of marine magnetotelluric data: Insights from a pilot study offshore northeastern Japan. *Phys Earth Planet Inter* 184(3–4):194–207
- Komori S, Utsugi M, Kagiya T, Inoue H, Chen C-H, Chiang H-T, Chao BF, Yoshimura R, Kanda W (2014) Hydrothermal system in the Tatun Volcano Group, northern Taiwan, inferred from crustal resistivity structure by audio-magnetotellurics. *Prog Earth Planet Sci* 1(1):1–14
- Krieger L, Peacock JR (2014) MTPy: a python toolbox for magnetotellurics. *Comput Geosci* 72:167–175
- Lin CC (1962) The quaternary of the Hualien Area—the quaternary of Taiwan. National Council on Science Development Research Report, 42 pp. **(in Chinese)**
- Lin Y-S, Chuang RY, Yen J-Y, Chen Y-C, Kuo Y-T, Wu B-L, Huang S-Y, Yang C-J (2019) Mapping surface breakages of the 2018 Hualien earthquake by using UAS photogrammetry. *Terr Atmos Ocean Sci.* <https://doi.org/10.3319/TAO.2018.12.09.02>
- Lin L-K, Hsu S-K, Tsai C-H, Yeh Y-C, Wang S-Y, Chen K-T, Chen S-C, Lin H-S (2021) Hualien Ridge: a tectonic ridge transitioning from plate collision to subduction. *Tectonophysics* 816:229010
- Schulze A, Bribach J, Jaekel K-H, Weber M (2003) The geophysical instrument pool Potsdam (GIPP)-state and impact on geophysical research. In: *Proceedings EGS-AGU-EUG Joint Assembly*, p 10324.
- Schwalenberg K, Edwards R (2004) The effect of seafloor topography on magnetotelluric fields: an analytical formulation confirmed with numerical results. *Geophys J Int* 159(2):607–621
- Selway K, Thiel S, Key K (2012) A simple 2-D explanation for negative phases in TE magnetotelluric data. *Geophys J Int* 188(3):945–958
- Shie Y-M (2017) Seismic reflection survey in the northern part of the Longitudinal Valley, the suture zone, in eastern Taiwan [Master: National Central University, p 104 **(in Chinese)**
- Shih TT, Chang JC, Hwang CE, Shih CD, Yang GS (1983) A geomorphological study of active fault in northern and eastern Taiwan. *Geogr Res* 9:20–72 **(in Chinese)**
- Shyu JBH, Chen C-F, Wu Y-M (2016) Seismotectonic characteristics of the northernmost Longitudinal Valley, eastern Taiwan: structural development of a vanishing suture. *Tectonophysics* 692:295–308
- Simpson F, Bahr K (2005) *Practical magnetotellurics*. Cambridge University Press
- Thong KD (2008) Coast effect on magnetotelluric data in Taiwan Island [Master: National Central University, p 100.
- Tikhonov AN (1950) On determining electric characteristics of the deep layers of the earth's crust. *Dokl Akad Nauk SSSR* 73:295–297
- Toyokuni G, Zhao D, Chen KH (2021) Structural control on the 2018 and 2019 Hualien earthquakes in Taiwan. *Phys Earth Planet Inter* 312:106673

- White A, Heinson G (1994) Two-dimensional electrical conductivity structure across the southern coastline of Australia. *J Geomagn Geoelectr* 46(12):1067–1081
- Wu B-L, Yen J-Y, Huang S-Y, Kuo Y-T, Chang W-Y (2019) Surface deformation of 0206 Hualien earthquake revealed by the integrated network of RTK GPS. *Terr Atmos Ocean Sci* 30:301–310
- Yamada M, Cho I, Kuo CH, Lin CM, Miyakoshi K, Guo Y, Hayashida T, Matsumoto Y, Mori J, Yen YT (2020) Shallow subsurface structure in the Hualien Basin and relevance to the damage pattern and fault rupture during the 2018 Hualien Earthquake. *Bull Seismol Soc Am* 110(6):2939–2952
- Yen J-Y, Lu C-H, Chung-Pai C, Hooper AJ, Chang Y-H, Liang W-T, Tsui-Yu C, Ming-Sheng L, Kun-Shan C (2011) Investigating active deformation in the northern Longitudinal Valley and City of Hualien in eastern Taiwan using persistent scatterer and small-baseline SAR interferometry. *Terr Atmos Ocean Sci* 22(3):2

Publisher's Note

Springer Nature remains neutral with regard to jurisdictional claims in published maps and institutional affiliations.

Submit your manuscript to a SpringerOpen[®] journal and benefit from:

- ▶ Convenient online submission
- ▶ Rigorous peer review
- ▶ Open access: articles freely available online
- ▶ High visibility within the field
- ▶ Retaining the copyright to your article

Submit your next manuscript at ► [springeropen.com](https://www.springeropen.com)
